Alterations in gap junction connexin43/connexin45 ratio mediate a transition from quiescence to excitation in a mathematical model of the myometrium

Rachel E. Sheldon[1,3,*], Chipo Mashayamombe[2,3], Shao-Qing Shi[4], Robert E. Garfield[4], Anatoly Shmygol[3], Andrew M. Blanks[3], and Hugo A. van den Berg[1]

[1]MOAC Doctoral Training Centre, University of Warwick, Coventry, CV4 7AL, UK

[2]Systems Biology Doctoral Training Centre, University of Warwick, Coventry, CV4 7AL, UK

[3]Division of Reproductive Health, Warwick Medical School, CV2 2DX, UK

[4]Department of Obstetrics and Gynecology, St. Joseph's Hospital and Medical Center, Phoenix, AZ

September 11, 2014

Abstract

The smooth muscle cells of the uterus contract in unison during delivery. These cells achieve coordinated activity via electrical connections called gap junctions, which consist of aggregated connexin proteins such as connexin43 and connexin45. The density of gap junctions governs the excitability of the myometrium (among other factors). An increase in gap junction density occurs immediately prior to parturition. We extend a mathematical model of the myometrium by incorporating the voltage-dependence of gap junctions that has been demonstrated in the experimental literature. Two functional subtypes exist, corresponding to systems with predominantly connexin43 and predominantly connexin45, respectively. Our simulation results indicate that the gap junction protein connexin45 acts as a negative

*To whom correspondence should be addressed. Email: R.E.Sheldon@warwick.ac.uk

modulator of uterine excitability, and hence, activity. A network with a higher proportion of connexin45 relative to connexin43 is unable to excite every cell. Connexin45 has much more rapid gating kinetics than connexin43 which we show limits the maximum duration of a local burst of activity. We propose that this effect regulates the degree of synchronous excitation attained during a contraction. Our results support the hypothesis that as labour approaches, connexin45 is down-regulated to allow action potentials to spread more readily through the myometrium.

Keywords: Uterus, Myometrium, Gap Junction, Mathematical model, Connexin45, Connexin43

1 Introduction

The myometrium, which makes up the bulk of the uterine wall in all species [1] (Figures SI 1a and SI 1b), is composed of interconnected smooth muscle cells, which form an excitable medium [2], *i.e.* a medium that is capable of propagating signals over relatively long distances with virtually no damping. In the myometrium, these propagating signals take the form of action potentials which trigger phasic contractions during labour [3]. These involve the rhythmic contraction and relaxation of the smooth muscle cells, giving rise to synchronised travelling waves throughout the uterus [4]. In humans the phasic contractions typically last for around a minute [5], whereas in rats they last for ∼68 seconds at term [6].

Throughout most of pregnancy, the myometrium remains quiescent, allowing the fœtus to develop undisturbed [7]. The myometrium undergoes major changes in the days leading up to labour [7]. In particular, as parturition approaches, the uterus becomes more excitable through an activation phase which involves molecular changes that lead to a decrease in time between subsequent contractions [8]. In humans, this interval decreases from ∼30 minutes to ∼2 minutes as pregnancy progresses [5, 8], whereas in rats contractions occur at 2.3-minute intervals at gestational day 19 and at 46-second intervals in active labour [6].

A key condition for the transition to excitability at the whole organ level is a change in connectivity between the myometrial smooth muscle cells [2]. The smooth muscle cells in the

myometrium are connected through a series of intercellular channels that allow the passage of ions and small molecules from one cell to another, each channel being made up of two components, one contributed by each cell [9].

As pregnancy progresses, the density of gap junctions on the cell-to-cell contact surfaces increases, which is thought to be one of many factors which instigate labour [2]. In the non-pregnant uterus of both rats and humans, gap junctions are either absent or present at low density [2, 10, 11]. At the time of delivery, gap junctions are present at a density of $\sim$1000 per cell in human tissue [12].

The ability of a myometrial network to achieve global excitation is strongly dependent on spatial heterogeneity of cell-to-cell connectivity [13]. Using a mathematical model of the myometrium based on FitzHugh-Nagumo dynamics [14, 15], we previously showed that a moderate degree of spatial heterogeneity allows excitation to spread throughout a network even if the same network would be quiescent when fully and uniformly connected. However, the coupling between cells was represented as a passive resistor, whereas in reality voltage-dependent gating is a well-established property of vertebrate gap junction channels [16–19]. This trans-junctional voltage-dependence is directly related to the connexin composition of the channel. Individual connexins exhibit different responses as a function of the potential difference between neighbouring cells; for example, connexin43 (Cx43) is relatively insensitive to the voltage difference, displaying only modest changes in conductance as the trans-junctional voltage is altered [20]. By contrast, connexin45 (Cx45) and connexin40 are highly sensitive to trans-junctional voltage differences [20–22]. The differences in connexin protein response to trans-junctional voltage are thought to be underpinned by different localisations of charged residues along the inner lining of the ion-conducting pore as well as different phosphorylation states [23, 24].

Miyoshi *et al.* [25] recorded gap-junctional currents between isolated pairs of rat myometrial cells, using the double-whole-cell voltage-clamp configuration (Figure SI 3). The cell pairs were found to exhibit one of two distinct relationships between conductance and voltage-dependence which occurred in equal proportions (Figure 1a). The so-called 'Type I' channels displayed a gradual increase from a normalised conductance of 0.2 to 1 with decreasing voltage difference.

At small trans-junctional voltages, there was very little change in conductance. By contrast, the 'Type II' channels showed a much sharper increase in conductance with decreasing voltage difference. A notable voltage-dependent change in conductance was observed even at small trans-junctional voltages. The authors observed that the Type I voltage-dependence relationship fit with the pattern expected for a tissue with predominantly Cx43 junction proteins. In addition, the Type II junction voltage-dependence appeared to be noticeably distinct from the connexin patterns observed before. The dependence of conductance on the trans-junctional voltage difference for Type II is more consistent with a Cx45 junction protein, a hypothesis that was further supported by the findings by Moreno *et al.* [26].

Here we investigate how the spread of excitation through a network is affected by incorporating voltage-dependent cell-to-cell couplings in the mathematical model. We adapt the voltage-dependent conductance relationships for both gap junction types identified by Miyoshi *et al.* [25]. The main qualitative effect is that conductance increases as the potential difference between the cells decreases. To isolate this "cut-off" effect, we initially model the voltage-dependence relationship as a simple step function. We subsequently compare our findings to more realistic voltage-conductance relationships in order to verify that the dominant qualitative effect is the "cut-off" point of activity.

Finally, we incorporate gating kinetics. We propose that the Type II gap junctions are not able to excite the network by themselves; a substantial proportion of Type I gap junctions is needed to spread activity effectively. The gating kinetics is much more rapid for Type II gap junctions in comparison with Type I junctions. The faster kinetics prevents the longer depolarisation propagating throughout the network, and so limits the excitability of the network. Accordingly, we suggest that relative proportion of Type I and Type II gap junctions is crucial for the modulation of activity in the excitable myometrial network.

Analysis of gene expression in rat models suggest that the expression of Cx45 is down-regulated in labour. We do not observe a change in the expression of Cx43 in the transition from pregnancy to labour. We therefore hypothesise that the relative proportion of Cx43 and Cx45 is crucial; Cx45 acts as a brake on activity in the uterus, and its down-regulation may be an

important step in the initiation of labour.

2 Methods

2.1 Mathematical modelling

We further develop a mathematical model of the myometrial smooth muscle network [13]. The network is constructed as a square lattice in which each node is connected to four others. Each simulated cell obeys FitzHugh-Nagumo dynamics. The FitzHugh-Nagumo model is a two-variable system which describes the excitation and relaxation of an excitable cell [28]. The model is an example of an excitation-relaxation oscillator due to its threshold properties in which a sufficiently large input of current is required for the cell to exhibit an excursion corresponding to excitation and relaxation. However, parameters can be chosen such that cells are autorhythmic [13], that is, the cells continually oscillate through the excitation-relaxation cycle without any external stimulus. FitzHugh-Nagumo is a simplification of the Hodgkin-Huxley model for spiking neurons [29, 30] and, as such, is often used in modelling excitable systems such as contractions of cardiac myocytes (for example, [31–33]).

Each node in the network is considered to be excitation-relaxation oscillator with a fast ("excitation") state variable v that corresponds to the transmembrane potential and a slow ("recovery") variable w that corresponds to gating kinetics which repolarise the excited cell. The following dimensionless ordinary differential equations describe this two-variable model:

$$\frac{d}{dt}v(t) = \frac{1}{\epsilon}(Bv(t)\,(1 - v(t))(v(t) - \alpha) - w(t) - w_0) + I\ , \tag{1a}$$

$$\frac{d}{dt}w(t) = v(t) - \gamma w(t) - v_0\ , \tag{1b}$$

where I is the input current and B, α, γ, w_0, v_0, and ϵ are positive parameters. The values shown in Table 1 are used in all simulations to generate a network of cells which require a suprathreshold current input to undergo an oscillation.

The equations were solved using an LSODE (Livermore Solver for Ordinary Differential Equa-

tions) approach through the NDSolve function in Mathematica. Results were numerically stable under variation in step size.

Each simulated cell is coupled to its four neighbours through resistors representing gap junctions (Figure SI 2a). A coupling constant K is assigned to each gap junction and defined as $K_{ij} = (C_i R_{ij})^{-1}$, where i and j are two neighbouring cells, C_i is the capacitance of cell i, and R_{ij} is the resistance between the two cells. The coupling K is therefore a rate constant, and is rendered dimensionless as follows. The FitzHugh-Nagumo model defines dimensionless time, t, as $t = R_1/\tau D$, where D is a damping coefficient that captures the inertia of the system due to the gating kinetics, as shown by FitzHugh [14], τ is dimensional time, and R_1 is the passive resistance of the nonlinear current device, represented as a tunnel diode by Nagumo *et al.* [15]. Accordingly, dimensionless coupling is defined as $D/R_1 K$ and denoted κ. The scaling of the remaining parameters is detailed in the Appendix and follows the derivation given by Keener and Sneyd [28].

Miyoshi *et al.* [25] identified two distinct relationships between the conductance of smooth muscle gap junctions and the voltage difference between two neighbouring myocytes (Figure 1a). We adapt these relationships to represent voltage-dependent gap junctions in terms of the coupling strength κ. Spatial heterogeneity is added to the system by introducing a probability p of a connection existing between any two adjacent cells, as previously described [13]. This parameter is referred to as the 'connectivity' of the network. The relative cluster size serves as a measure of the proportion of cells in the network that become excited: if all cells are excited, the relative cluster size equals 1, whereas if no cells become excited, it is 0.

2.1.1 Step function model

The simplest way to represent the voltage-dependence is by means of a step function (Figure 1b). For cells with a small voltage difference, the normalised gap-junctional conductance is set to be 1 whereas for cells with a large voltage difference, the normalised gap-junctional conductance is 0.2 (the base value determined by Miyoshi *et al.* [25]). We use the term *gap-junctional conductance bandwidth* to mean the range of voltage differences for which the gap-junctional

conductance equals 1. The voltage differences are scaled from unit-bearing values to the dimensionless FitzHugh-Nagumo model values. To facilitate numerical analysis, the step function is smoothed, as follows (Figures SI 4a and SI 4b):

$$\text{Relative conductance} = 0.6 + \frac{0.4 \times (\psi/2 - |((v_i(t) - v_j(t)) \times \lambda)|)}{\sqrt{1 + (\psi/2 - |((v_i(t) - v_j(t)) \times \lambda)|)^2}}, \tag{2}$$

where the indices i and j represent adjacent cells, λ is the scaling required to convert between physiological values and the FitzHugh-Nagumo model values, and ψ is the gap-junctional conductance bandwidth. The relative conductance is multiplied by the coupling strength κ. In the majority of simulations, $\kappa = 1$; however, we also present some results with $\kappa = 0.76$ to facilitate comparison with previous results in which we demonstrated the importance of heterogeneity [13].

Scaling is based on a typical rat myometrial cell in accordance with Miyoshi *et al.* [25]. The membrane potential of a rat myometrial cell increases from -45 mV to $+10$ mV during the upstroke of a full action potential, corresponding to an excursion of 55 mV. In the non-dimensionalised model, the size of the excursion is 3.52278. Accordingly, λ is taken to be 55/3.52278. To vary the width of the gap-junctional conductance band ψ is selected from the range 40 mV to 200 mV (twice the difference to zero, which lies at the midpoint). The value of ψ then dictates the voltage difference values over which the conductance of the gap junction equals 1. For example, $\psi = 120$ mV sets the conductance to 1 over a voltage difference of ± 60 mV, as illustrated in Figure 1b.

To check the model against our previous findings, the bandwidth is set to a sufficiently high value such that the relative conductance remains 1 over the entire voltage range of the action potential. The proportion of cells that become excited as a function of connectivity p reproduce our previous results; see Figure SI 5 for more details. With a coupling strength $\kappa = 0.76$, we replicate our previous scenarios in which spatial heterogeneity proved to be crucial in exciting the network (Figure SI 6).

2.1.2 Symmetrical Miyoshi model

Miyoshi *et al.* [25] proposed the following empirical equation for the conductance-voltage relationship:

$$g(V_j) = \frac{(1 - G_{\min})}{1 + \exp\{-A(V_j - V_h)\}} + G_{\min}, \tag{3}$$

where g is the normalised conductance of the gap junction, V_j is the voltage difference across the gap junction, $G_{\min}$ is the minimum value of the conductance, V_h is the half inactivation voltage (mV) at which the conductance is reduced by $(1 - G_{\min})/2$, and A is a slope factor ($(\text{mV})^{-1}$). The authors identified two distinct types of voltage-dependent gap junctions with the parameters given in Table 2. The relationship between the voltage gradient and gap-junctional conductance is shown for both types in Figure 1a.

To investigate the effect of the width of the gap-junctional conductance band, we model the Type I relationship by means of the bandwidth parameter ψ that allows us to scale the Type I relationship to resemble the Type II relationship. We employ a symmetrical version by taking the absolute value of the voltage and using the positive values that Miyoshi *et al.* [25] obtained for the Boltzmann fit, as shown in the following equation:

$$g(V_j) = \frac{(1 - G^+_{\min})}{1 + \exp\left\{-A^+(|V_j \times \lambda \times 110/\psi| - V^+_h)\right\}} + G^+_{\min}, \tag{4}$$

where λ is the scaling required to convert between physiological values and FitzHugh-Nagumo values; and ψ is the required width of the gap-junctional conductance band. For instance, $\psi = 110$ mV will give Type I, and $\psi = 40$ mV will give Type II. The scaling parameter $\lambda = 55/3.52278$, as before. A pictorial representation of the symmetrical Miyoshi model [25] is shown in Figure 1c.

We checked the model against our previous results by setting the bandwidth to a high value in order to attain a relative conductance of 1 over the action potential voltage range (Figure SI 7).

2.1.3 Symmetrical Miyoshi model with gating kinetics

The dependence of conductance on trans-gap-junctional voltage as described in the previous section is non-dynamic, *i.e.* the gating kinetics is sufficiently rapid to justify a quasi-instantaneous model. We now turn to more realistic gating kinetics. In the first instance, voltage-dependence of the time constant is ignored, giving rise to the following ordinary differential equation:

$$\frac{d}{dt}g = \frac{1}{\tau_g}(\bar{g}(V_j) - g) \ , \tag{5}$$

where g is the conductance of an individual gap junction, τ_g is the gap-junctional time constant, and $\bar{g}$ is the steady-state conductance dependent on the trans-junctional voltage V_j as considered in Sections 2.1.1 and 2.1.2. A complete excitation-relaxation cycle in the FitzHugh-Nagumo model lasts for 18.6849 dimensionless units (the time at which the cell is able to become re-excited) and we assume an action potential burst in the rat lasts for around 30 seconds. Therefore to convert from dimensionless time to seconds, we multiply the dimensionless time by 30/18.6849.

We next consider a model in which the time constant τ_g is dependent on the potential difference between neighbouring cells. The voltage-dependence relationship for the time constants is derived from Miyoshi *et al.* [25] by considering the gap-junctional current response after 5-second step pulses of voltages in the range ±90 mV (Figures 2a and 2b, respectively). The Type I and Type II gap junctions exhibit distinct relationships, given in Figure 2. An exponential equation is fitted using the least-squares criterion to each current response in order to determine the time constant for each voltage difference. A Gaussian is then fitted using the least-squares criterion to the time constants giving voltage-dependent time constant relationships as follows:

$$\text{Time constant} = a \times e^{-(V_j^2/2b^2)} + c, \tag{6}$$

where V_j is the trans-junctional voltage, $a = 9.39726$, $b = 23.9757$, and $c = 0.60274$ for Type I, and $a = 9.41999$, $b = 16.799$, and $c = 0.580013$ for Type II (Figure 3). We are not able to obtain good estimates of the rate of decay near 0 mV since the time constant here substantially

exceeds the duration of the experiment.

2.2 Experimental methods

We employed rat models in order to investigate the changes in expression of Cx43 and Cx45 in the myometrium between gestational ages of 19 $\frac{1}{4}$ and 22 days. Detailed experimental methods are provided in Section SI 1.1.

3 Results

The effect of varying the gap-junctional conductance band width is studied first. We then examine cases in which the conductance relaxes to a steady state over a certain period of time. In more sophisticated simulations, the time constant is dependent on the voltage difference between neighbouring cells.

3.1 Minimal gap-junctional conductance bandwidth

Numerical simulations with the step function model indicate that there is a critical minimal gap-junctional conductance band below which global excitation cannot be achieved (Figure 4a). For conductance bandwidths of 100 mV, 80 mV, 60 mV, and 40 mV, full activity is observed with a fully connected lattice. However, once the conductance bandwidth drops below 40 mV, all activity disappears and only the perturbed cell is capable of being excited. The transition from excitation to quiescence is quite steep and takes place over a very small range of bandwidth values: between 40 mV and 39 mV (Figure 4b). Simulations with several lattice sizes indicate that this transition has the character of a discontinuous phase transition in the limit of infinite lattice size (see Figures SI 8 and SI 9 for further details).

The critical value of the bandwidth is loacted between the apparent bandwidth values of Type I and Type II gap junctions as described by Miyoshi *et al.* [25] (Figure 5a). This strongly suggests that physiological significance can be attached to the qualitative difference between

bandwidths for which no global excitation is achieved, and those bandwidths that permit global excitation.

To assess the hypothesis that the threshold bandwidth value is significant, we ran simulations in which cell-to-cell couplings were randomly assigned the bandwidth corresponding to Type I or Type II, using probabilities of inter-cell connections of 0.4, 0.6, 0.8, and 1. The relative cluster size increases with the proportion of Type I gap junctions (Figure 6), with a steep increase between ratios of Type II to Type I gap junctions of 0.4 and 0.6. This qualitative result is also found with lower connection probabilities. As the connectivity of the lattice is decreased, the transition values shift in favour of a larger proportion of Type I gap junctions.

The qualitative results obtained with the step function model were repeated in a model which more closely represented the shape of the Type I and Type II Miyoshi *et al.* [25] fits (see Section 2.1.2). There is a minimum gap-junctional conductance bandwidth beyond which no excitation can take place, and a clear transition between excited and quiescent states. The results of this simulation are detailed in Figures SI 10 and SI 11.

Network activity depends on the connectivity p and the ratio of Type II to Type I gap junctions. Figure 7 suggest that there is a defined set of conditions that promote network excitation. The majority of parameter combinations result in no activity. However, a network with high connectivity and a higher proportion of Type I gap junctions relative to Type II gap junctions maximises the likelihood of near full activity.

3.2 The effect of gating kinetics

Here we examine the symmetrical Miyoshi model with voltage-gated gap junctions using a fixed time constant. The excitability of a network with exclusively Type I gap junctions is unaffected by the value of the time constant — there is always full activity at full connectivity (Figure 8a). By contrast, the time constant is a key parameter in a network with Type II gap junctions. With a small time constant, Type II gap junctions are unable to propagate any activity, as before. However, as the time constant is increased, the relationship between

connectivity and relative cluster size assumes one of two distinct forms (Figure 8b). For time constants between 0.87 and 1.49 seconds (0.54 and 0.93 in dimensionless units) the relationship follows a bell-shaped curve, indicative of the importance of spatial heterogeneity in exciting the network. For time constants larger than 1.51 seconds (0.94 in model values) the relationship follows a sigmoidal curve in which full connectivity corresponds to full excitation. These results are summarised in Table 3.

Comparisons are drawn between the time constant thresholds identified above, and the time constant relationship with voltage difference for Type II gap junctions (Figure 3b). For a voltage difference greater than ± 50 mV, excitation in the network is not possible. For voltage differences smaller than ± 35 mV, excitation is always possible. When the voltage difference is between ± 35 mV and ± 50 mV, spatial heterogeneity in connections is essential to obtain excitation in the network.

Finally, we examine a network with varying proportions of Type I and Type II gap junctions. As before, cell-to-cell couplings were randomly assigned the bandwidth corresponding to Type I or Type II. In addition, the voltage-dependent time constants corresponding to the chosen bandwidth are incorporated into the model using the Gaussian fit detailed in Equation 6. Type II gap junctions remain unable to produce full network excitation even at full connectivity (Figure 9). A small influence of spatial heterogeneity is apparent for networks with exclusively Type II gap junctions. Around 20% of cells are able to become excited with connectivities in the range 0.6 – 0.8. Type I gap junctions are unaffected by the switch to voltage-dependent time constants. The cells in the network are still able to exhibit full activity with full connectivity. As the connectivity is reduced, so is the excitation.

3.3 Experimental results

Transcriptomics data suggest that expression of connexin45 (Cx45) in the inner myometrium is substantially lower on gestation day 22 (in labour) as compared to gestation day 19.25 (Figure 10a). On the other hand, there does not appear to be a difference in connexin43 (Cx43) expression between these two points in time in either the inner or outer myometrium (Fig-

ure 10b). Taken together, these data would suggest an increase of the Cx43:Cx45 ratio, *i.e.* a relative enrichment of Cx43.

4 Discussion

Our findings suggest that the relative proportions of connexin43 (Cx43) and connexin45 (Cx45) are vital in initiating contractions in the myometrium during parturition. We build on the results obtained by Miyoshi *et al.* [25] to show that global excitation can be attained in a model network relying solely on Cx43 proteins, whereas this is not the case for a system using only Cx45. In addition, we develop a model in which the conductance of a gap junction is dynamic and has a voltage-dependent time constant, Cx45 having faster gating kinetics than Cx43. We demonstrated that this time constant is a key factor in determining whether global excitation can be achieved. At shorter time constants, heterogeneity in the density of gap junction connections plays a more prominent role in deciding whether activity can spread.

In rodents (as in most mammals, but not humans [34]), the myometrium can be divided into two distinct layers of smooth muscle: the inner circular layer and the outer longitudinal layer [35]. Our experimental data indicate down-regulation of Cx45 expression in the rat as labour approaches, in contrast to Cx43 expression where no change at the end of pregnancy appears to be evident. Chan *et al.* [36] found similar results in human myometrium, analysing the RNA of myometrial samples from pregnant women (5 from women in labour, and 5 from women at full term, but not in labour). These authors showed that Cx43 expression remains unchanged between the two sample groups, whereas Cx45 expression is significantly down-regulated in the "in labour" group in comparison with the "not-in-labour" group (Figure SI 12). These results are in accordance with our data, which furthermore suggest that the significant changes found by Chan *et al.* [36] were due to changes in expression taking place in the inner myometrium as opposed to the outer myometrium. Our model simulations show that an elevated proportion of Cx43 proteins is a key factor in modulating conductance. This accords well with results obtained by Döring *et al.* [37] and Tong *et al.* [38], who found that in a Cx43 knock-out mouse, the lack of intracellular myometrial coupling results in weaker contractions and delayed labour.

These various lines of evidence strongly suggest that the Cx43:Cx45 ratio is instrumental in controlling the global excitability of the myometriocyte network.

The connexin protein Cx45 plays an important role in cardiac myocytes; it is found in the atrioventricular (AV) node and the adjoining His bundles [39, 40]. While Cx45 is not essential for continued survival in the adult mouse [40], Cx45 knock-out mice die from heart failure *in utero* [41, 42]. Without Cx45, contractions initiated in the AV node are not coordinated with the contractions in the ventricles; Cx45 may play a similar role in the myometrium, *i.e.*, to inhibit contractions until the development of the baby has advanced sufficiently for delivery. The inviability of Cx45 knock-out mouse embryos [41, 42] precludes a test of this hypothesis *in vivo*. However, Cx45 knock-out *in vitro* studies could be used to demonstrate the development of global network events.

Voltage-dependent gap junctions have previously been considered in mathematical models [43, 44]. Baigent *et al.* [45, 46] and Donnell *et al.* [47] considered a two-cell model coupled by a dynamic gap junction which resides in one of three states, giving insights into cell connections on a local scale, emphasising channel kinetics and ionic flows in great detail. By contrast, the present model focuses on overall excitability of the network as a function of spatial heterogeneity of the functional properties of the gap junctions, rather than on the propagation of activity wave fronts and the spatial patterning of such fronts; these aspects have been considered elsewhere [4, 33, 48, 49]. Whereas we considered the global activation threshold in a electrotonically coupled smooth muscle syncytium, a general argument regarding the all-or-none character of synaptically coupled networks, such as the central nervous system, was advanced by Ashby *et al.* [50].

The present work has not considered heteromeric gap junction channels with both Cx45 and Cx43 proteins. We assumed that the relationships given by Miyoshi *et al.* [25] correspond to homomeric gap junction channels. Martinez *et al.* [51] demonstrated that these two gap junction proteins are coexpressed in cardiac cells, and that homomeric channels of either Cx45 or Cx43 have different unitary conductances. A heteromeric gap junction channel might exhibit non-symmetrical behaviour; this will require further experimental studies in order to inform

our model.

We do not report an increase in Cx43 expression in the rat between day $19\frac{1}{4}$ and day 22. This finding is in keeping with the literature in that the rise in Cx43 occurs prior to parturition (4 days before term in the rat). Cx43 proteins are stored in vesicles and only trafficked to the membrane gap junctions when labour commences, so causing a increase in functional expression in labour, but not an increase in gene expression in the tissue [11, 52–55]. Studies using immunohistochemistry and western blot analysis have demonstrated the functional increase in Cx43 expression at term, as well as a decrease in Cx45 [56, 57]. Albrecht *et al.* [56] suggested that the ratio of Cx43 to Cx45 might be crucial for increased network connectivity associated with the initiation of labour, which is in agreement with our finding that relative numbers of Cx43 and Cx45 are a key permissive factor — Cx45 effectively acting as a brake on contractile activity in the uterus. As parturition approaches, Cx45 becomes down-regulated, allowing contractions to increase in strength and frequency.

5 Acknowledgements

RES is grateful to EPSRC for a PhD studentship through the MOAC Doctoral Training Centre at the University of Warwick: grant number EP/F500378/1.

CM gratefully acknowledges funding for a PhD studentship from the BBSRC through the Systems Biology Doctoral Training Centre at the University of Warwick: grant number BB/G530233/1.

References

[1] Putz, R. & Pabst, R. 1989 *Sobotta - Atlas of Human Anatomy.* 14^{th} ed. Munich: Elsevier.

[2] Garfield, R.E., Sims, S. & Daniel, E.E. 1977 Gap junctions: their presence and necessity in myometrium during parturition. *Science* **198** (4320), 958–960. (DOI: 10.1126/science.929182)

[3] Parkington, H.C., Tonta, M.A., Davies, N.K., Brennecke, S.P. & Coleman, H.A. 1999

Hyperpolarization and slowing of the rate of contraction in human uterus in pregnancy by prostaglandins E_2 and $F_{2\alpha}$: involvement of the Na^+ pump. *Journal of Physiology* **514** (1), 229–243. (DOI: 10.1111/j.1469-7793.1999.229af.x)

[4] Singh, R., Xu, J., Garnier, N.G., Pumir, A. & Sinha, S. 2012 Self-organized transition to coherent activity in disordered media. *Phys. Rev. Lett.* **108** (6), 068102. (DOI: 10.1103/PhysRevLett.108.068102)

[5] Maeda, K. 2013 Uterine contractions in normal labor developed by a positive feed-back and oscillation. *J. Health Med. Informat.* **4** (3), 130. (DOI: 10.4172/2157-7420.1000130)

[6] Buhimschi, C., Boyle, M.B., Saade, G.R. & Garfield, R.E. 1998 Uterine activity during pregnancy and labor assessed by simultaneous recordings from the myometrium and abdominal surface in the rat. *Am. J. Obstet. Gynecol.* **178** (4), 811–822. (DOI: 10.1016/S0002-9378(98)70498-3)

[7] Challis, J.R.G., Matthews, S.G., Gibb, W. & Lye, S.J. 2000 Endocrine and paracrine regulation of birth at term and preterm. *Endocrine Reviews* **21** (5), 514–550. (DOI: 10.1210/er.21.5.514)

[8] Parkington, H.C., Tonta, M.A., Brennecke, S.P. & Coleman, H.A. 1999 Contractile activity, membrane potential, and cytoplasmic calcium in human uterine smooth muscle in the third trimester of pregnancy and during labor. *Am J Obstet Gynecol* **181** (6), 1445-51. (DOI: 10.1016/S0002-9378(99)70390-X)

[9] Kumar, N.M. & Gilula, N.B. 1996 The gap junction communication channel. *Cell* **84** (3), 381–388. (DOI: 10.1016/S0092-8674(00)81282-9)

[10] Garfield, R.E., Sims, S.M., Kannan, M.S. & Daniel, E.E. 1978 Possible role of gap junctions in activation of myometrium during parturition. *Am. J. Physiol.* **235** (5), C168–C179.

[11] Risek, B., Guthrie, S., Kumar, N. & Gilula, N.B. 1990 Modulation of gap junction transcript and protein expression during pregnancy in the rat. *J. Cell Biol.* **110** (2), 269–282.

[12] Garfield, R.E., Blennerhassett, M.G., Miller, S.M. 1988 Control of myometrial contractility: role and regulation of gap junctions.. *Oxf. Rev. Reprod. Biol.* **10**, 436–490.

[13] Sheldon, R.E., Baghdadi, M., McCloskey, C., Blanks, A.M., Shmygol, A. & van den Berg, H.A. 2013 Spatial heterogeneity enhances and modulates excitability in a mathematical model of the myometrium. *J R Soc Interface* **10** (86). (DOI: 10.1098/rsif.2013.0458)

[14] FitzHugh, R. 1961 Impulses and physiological states in theoretical models of nerve membrane. *Biophys J* **1** (6), 445–466. (DOI: 10.1016/S0006-3495(61)86902-6)

[15] Nagumo, J., Arimoto, S. & Yoshizawa, S. 1962 An active pulse transmission line simulating nerve axon. *Proceedings of the IRE* **50** (10), 2061 – 2070. (DOI: 10.1109/JRPROC.1962.288235)

[16] Spray, D.C., Harris, A.L. & Bennett, M.V.L. 1979 voltage-dependence of junctional conductance in early amphibian embryos. *Science* **204** (4391), 432 – 434. (DOI: 10.1126/science.312530)

[17] Spray, D.C., Harris, A.L. & Bennett, M.V.L. 1981 Equilibrium properties of a voltage-dependent junctional conductance. *J. Gen. Physiol.* **77** (1), 77 – 93. (DOI: 10.1085/jgp.77.1.77)

[18] Harris, A.L., Spray, D.C. & Bennett, M.V.L. 1981 Kinetic properties of a voltage-dependent junctional conductance. *J. Gen. Physiol.* **77** (1), 95 – 117. (DOI: 10.1085/jgp.77.1.95)

[19] Wang, H-Z., Li, J., Lemanski, L.F. & Veenstra, R.D. 1992 Gating of mammalian cardiac gap junction channels by trans-junctional voltage. *Biophys. J.* **63** (1), 139 – 151. (DOI: 10.1016/S0006-3495(92)81573-4)

[20] Veenstra, R.D., Wang, H-Z., Westphale, E.M. & Beyer, E.C. 1992 Multiple connexins confer distinct regulatory and conductance properties of gap junctions in developing heart. *Circ. Res.* **71** (5), 1277 – 1283. (DOI: 10.1161/01.RES.71.5.1277)

[21] Veenstra, R.D., Wang, H-Z., Beyer, E.C. & Bring, P.R. 1994 Selective dye and ionic

permeability of gap junction channels formed by connexin45. *Circ. Res.* **75** (3), 483 – 490. (DOI: 10.1161/01.RES.75.3.483)

[22] Beblo, D.A., Wang, H-Z., Beyer, E.C., Westphale, E.M. & Veenstra, R.D. 1995 Unique conductance, gating, and selective permeability properties of gap junction channels formed by connexin40. *Circ. Res.* **77** (4), 813 – 822. (DOI: 10.1161/01.RES.77.4.813)

[23] Verselis, Y.K., Ginter, C.S. & Bargiello, T.A. 1994 Opposite voltage gating polarities of two closely related connexins. *Nature* **368** (6469), 348 – 351. (DOI: 10.1038/368348a0)

[24] Moreno, A.P., Fishman, G.I. & Spray, D.C. 1992 Phosphorylation shifts unitary conductance and modifies voltage-dependent kinetics of human connexin43 gap junction channels. *Biophsy. J.* **62** (1), 51 – 53. (DOI: 10.1016/S0006-3495(92)81775-7)

[25] Miyoshi, H., Boyle, M.B., MacKay, L.B. & Garfield, R.E. 1996 Voltage-clamp studies of gap junctions between uterine muscle cells during term and preterm labor. *Biophysical Journal* **71** (3), 1324–1334. (DOI: 10.1016/S0006-3495(96)79332-3)

[26] Moreno, A.P., Laing, J.G., Beyer, E.C. & Spray, D.C. 1995 Properties of gap junction channels formed of connexin 45 endogenously expressed in human hepatoma (SKHep1) cells. *Am. J. Physiol Cell Physiol* **268** (2), C366 – C365.

[27] Nielsen, M.S., Axelsen, L.N., Sorgen, P.L., Verma, V., Delmar, M. & Holstein-Rathlou, N.H. 2012 Gap junctions. *Compr. Physiol.* **2** (3), 1981–2035. (DOI: 10.1002/cphy.c110051)

[28] Keener, J. & Sneyd, J. 1998 Excitability. In *Mathematical Physiology* (ed. J. E. Marsden, L. Sirovich & S. Wiggins), pp.116–159. New York: Springer-Verlag.

[29] Hodgkin, A.L., Huxley, A.F. & Katz, B. 1952 Measurement of current-voltage relations in the membrane of the giant axon of *Loligo*. *J Physiol* **116**, 242–228.

[30] Hodgkin, A.L. & Huxley, A.F. 1952d A quantitative description of membrane current and its application to conduction and excitation in nerve. *J Physiol* **177**, 500–544.

[31] Zhang, H. & Holden, A.V. 1995 Chaotic meander of spiral waves in the FitzHugh-Nagumo

system. *Chaos, Solitons & Fractals* **5** (3–4), 661–670. (DOI: 10.1016/0960-0779(93)E0048-G)

[32] Aliev, R.R. & Panfilov, A.V. 1996 A simple two-variable model of cardiac excitation. *Chaos, Solitons & Fractals* **7** (3), 292–301. (DOI: 0.1016/0960-0779(95)00089-5)

[33] Benson, A.P., Clayton, R.H., Holden, A.V., Kharche, S. & Tong, W.C. Endogenous driving and synchronization in cardiac and uterine virtual tissues: bifurcations and local coupling. *Phil Trans R Soc A* **364**, 1313–1327. (DOI: 10.1098/rsta.2006.1772)

[34] Weiss, S., Jaermann, T., Schmid, P., Staempfli, P., Boesiger, P., Niederer, P., Caduff, R. & Bajka, M. 2006 Three-dimensional fiber architecture of the nonpregnant human uterus determined ex vivo using magnetic resonance diffusion tensor imaging. *Anat Rec A Discov Mol Cell Evol Biol* **288**, 84–90. (DOI: 10.1002/ar.a.20274)

[35] Brody, J.R. & Cunha, G.R. 1989 Histologic, morphometric, and immunocytochemical analysis of myometrial development in rats and mice: II. Effects of DES on development. *Am J Anat* **186**, 21–42. (DOI: 10.1002/aja.1001860103)

[36] Chan, Y-W., van den Berg, H.A., Moore, J.D., Quenby, S. & Blanks, A.M. 2014 Assessment of myometrial transcriptome changes associated with spontaneous human labour by high throughput RNA-seq. *Exp. Physiol.* **99** (3), 510–524. (DOI: 10.1113/expphysiol.2013.072868)

[37] Döring, B., Shynlova, O., Tsui, P., Eckardt, D., Janssen-Bienhold, U., Hofmann, F., Feil, S., Feil, R., Lye, S.J. & Willecke, K. 2006 Ablation of connexin43 in uterine smooth muscle cells of the mouse causes delayed parturition. *J. Cell Sci.* **119** (Pt 9), 1715–1722. (DOI: 10.1242/jcs.02892)

[38] Tong, D., Lu, X., Wang, H-W., Plante, I., Lui, E., Laird, D.W., Bai, D. & Kidder, G.M. 2009 A dominant loss-of-function GJA1 (Cx43) mutant impairs parturition in the mouse. *Biol. Reprod.* **80** (6), 1099-1106. (DOI:10.1095/biolreprod.108.071969)

[39] Gourdie, R.G. & Lo, C.W. 1999 Cx43 (α1) gap junctions in cardiac development and disease. *Curr Top Membr* **49**, 581 – 602. (DOI: 10.1016/S0070-2161(08)61030-8)

[40] Frank, M., Wirth, A., Andrié, R.P., Kreuzberg, M.M., Dobrowolski, R., Seifert, G., Offermanns, S., Nickenig, F., Willecke, K. & Schrickel, J.W. 2012 Connexin45 provides optimal atrioventricular nodal conduction in the adult mouse heart. *Circ. Res.* **111** (12), 1528 – 1538. (DOI: 10.1161/CIRCRESAHA.112.270561)

[41] Kumai, M., Nishii, K., Nakamura, J.I., Takeda, N., Suzuki, M. & Shibata, Y. 2000 Loss of connexin45 causes a cushion defect in early cardiogenesis. *Development* **127** (16), 3501 – 3512.

[42] Krüger, O., Plum, A., Kim, J-S., Winterhager, E., Maxeiner, S., Hallas, S., Kirchhoff, S., Traub, O., Lamers, W.H. & Willecke, K. 2000 Defective vascular development in connexin 45-deficient mice. *Development* **127** (19), 4179 – 4193.

[43] Vogel, R. & Weingart, R. 1998 Mathematical model of vertebrate gap junctions derived from electrical measurements on homotypic and heterotypic channels. *J Physiol.* **510** (1), 177 – 189. (DOI: 10.1111/j.1469-7793.1998.177bz.x)

[44] Chen-Izu, Y., Moreno, A.P. & Spangler, R.A. 2001 Opposing gates model for voltage gating of gap junction channels. *Am J Physiol Cell Physiol* **281** (5), C1604 – C1613.

[45] Baigent, S., Stark, J. & Warner, A. 1997 Modelling the effect of gap junction nonlinearities in systems of coupled cells. *J. Theor. Biol.* **186** (2), 223 – 229. (DOI: 10.1006/jtbi.1996.0351)

[46] Baignet, S. 2003 Cells coupled by voltage-dependent gap junctions: the asymptotic dynamical limit. *BioSystems* **68** (2–3), 213 – 222. (DOI: 10.1016/S0303-2647(02)00097-7)

[47] Donnell, P., Baigent, S. & Banaji, M. 2009 Monotone dynamics of two cells dynamically coupled by a voltage-dependent gap junction. *J. Theor. Biol.* **261** (1), 120 – 125. (DOI: 10.1016/j.jtbi.2009.07.012)

[48] Barkley, D. 1991 A model for fast computer simulation of waves in excitable media. *Physica D* **49**, 61–70. (DOI: 10.1016/0167-2789(91)90194-E)

[49] Bub, G., Shrier, A. & Glass, L. 2002 Spiral wave generation in heterogeneous excitable media. *Phys. Rev. Lett.* **88**, 058101. (DOI: 10.1103/PhysRevLett.88.058101)

[50] Ashby, W.R., von Foerster, H. & Walker, C.C. 1962 Instability of pulse activity in a net with threshold. *Nature* **196**, 561 – 562. (DOI: 10.1038/196561a0)

[51] Martinez, A.D., Hayrapetyan, V., Moreno, A.P. & Beyer, E.C. 2002 Connexin43 and connexin45 form heteromeric gap junction channels in which individual components determine permeability and regulation. *Circ. Res.* **90** (10), 1100 – 1107. (DOI: 10.1161/01.RES.0000019580.64013.31)

[52] Winterhager, E., Stutenkemper, R., Traub, O., Beyer, E. & Willecke, K. 1991 Expression of different connexin genes in rat uterus during decidualization and at term. *Eur. J. Cell. Biol.* **55** (1), 133 – 142.

[53] Hendrix, E.M., Mao, S.J.T., Everson, W. & Larsen, W.J. 1992 Myometrial connexin 43 trafficking and gap junction assembly at term and preterm labor. *Mol. Reprod. Dev.* **33** (1), 27 – 38. (DOI: 10.1002/mrd.1080330105)

[54] Tabb, T., Thilander, G., Grover, A., Hertzberg, E. & Garfield, R.E. 1992 An immunochemical and immunocytological study of the increase in myometrial gap junctions (and connexin 43) in rats and humans during pregnancy. *Am. J. Obstet. Gynecol.* **167** (2), 559 – 567. (DOI: 10.1016/S0002-9378(11)91453-7)

[55] Garfield, R.E. & Hayashi, R.H. 1981 Appearance of gap junctions in the myometrium of women during labor. *Am. J. Obstet. Gynecol.* **140** (3), 958 – 959.

[56] Albrecht, J.L., Atal, N.S., Tadros, P.N., Orsino, A., Lye, S.J., Sadovsky, Y & Beyer, E. 1996 Rat uterine myometrium contains the gap junction protein connexin45, which has a differing temporal expression pattern from connexin43. *Am. J. Obstet. Gynecol.* **175**, 853 – 858. (DOI: 10.1016/S0002-9378(96)80012-3)

[57] Kilarski, W.M., Semik, D., Roomans, G.M., Ulmstem, U. & Severs, N.J. 1998 Immunohistochemical analysis of connexins 26, 32 and 43 in rat uterus during late pregnancy:

lack of connexin 26 in the myometrium. *Histochemical Journal* **30**, 307 – 316. (DOI: 10.1023/A:1003224225975)

[58] Andrews, S. *FastQC A Quality Control tool for High Throughput Sequence Data.* http://www.bioinformatics.babraham.ac.uk/projects/fastqc/ (Accessed 24^{th} September 2013)

[59] Kim, D., Pertea, G., Trapnell, C., Pimentel, H., Kelley, R. & Salzberg, S.L. 2013 TopHat2: accurate alignment of transcriptomes in the presence of insertions, deletions and gene fusions. *Genome Biology* **14**: R36. (DOI: 10.1186/gb-2013-14-4-r36)

[60] Gibbs, R.A., Weinstock, G.M., Metzker, M.L. *et al.* 2004 Genome sequence of the Brown Norway rat yields insights into mammalian evolution. *Nature* **428** (6982), 493 – 521. (DOI: 10.1038/nature02426)

[61] Li, H., Handsaker, B., Wysoker, A., Fennell, R., Ruan, J., Homer, N., Marth, G., Abecasis, G., Durbin, R. & 1000 Genome Project Data Processing Subgroup. 2009 The sequence alignment/map format and SAMtools. *Bioinformatics* **25** (16), 2078 – 2079. (DOI: 10.1093/bioinformatics/btp352)

[62] Thorvaldsdóttir, H., Robinson, J.T. & Mesirov, J.P. 2012 Integrative genomics viewer (IGV): high-performance genomics data visualization and exploration. *Brief Bioinform.* **14** (2), 178 – 192. (DOI: 10.1093/bib/bbs017)

[63] Patro, R., Mount, S.M. & Kingsford, C. 2014 Sailfish enables alignment-free isoform quantification from RNA-seq reads using lightweight algorithms. *Nature Biotechnology* **32**, 462 – 464. (DOI: 10.1038/nbt.2862)

[64] Wagner, G.P., Kin, K. & Lynch, V.J. 2012 Measurement of mRNA abundance using RNA-seq data: RPKM measure is inconsistent among samples. *Theory in Biosciences* **131** (4), 281 – 285. (DOI: 10.1007/s12064-012-0162-3)

6 Figures

Figure 1: (a) Relationship between conductance and voltage difference between neighbouring cells as published by Miyoshi *et al.* [25]. The blue line shows the Type I gap junction relationship identified; the red line shows the Type II gap junction relationship identified. Points show experimental conductances determined by Miyoshi *et al.* [25]. The lines represent Boltzmann curve fits to the data (Equation 3); (b) Step function describing the relationship between voltage difference and gap-junctional conductance. A value $\psi = 120$ corresponds to a conductance of 1 over a voltage difference of ± 60 mV; (c) Symmetrical curves for the Type I relationship (blue) and the Type II relationship (red) identified by Miyoshi *et al.* [25]. Type II is determined from Type I by a change in the parameter ψ in Equation 4.

Figure 2: Gap junction current responses over time following step pulses of voltages between $\pm$ 90 mV. Pulses of ± 90 mV are shown in red, ± 70 mV in orange, ± 50 mV in yellow, ± 30 mV in green, and ± 10 mV in blue. Lines shown are curve fits to experimental data published by Miyoshi *et al.* [25]. (a) The Type I response; (b) The Type II response.

Figure 3: (a) The relationships between voltage difference between neighbouring cells and the time constant of the gap junctions. The Type I relationship is shown in red, and the Type II relationship is shown in blue; (b) Comparison of voltage difference between neighbouring cells and the time constant of the gap junction for Type II junctions (as in Figure 3). The red shaded region indicates time constants for the Type II junctions in which no excitation is possible. The blue shaded region indicates time constants for the Type II junctions in which spatial heterogeneity is necessary for excitation to take place.

Figure 4: Relative cluster size versus connectivity p for a lattice with gap-junctional conductance related to voltage-dependence with a step function. Points show mean $\pm$ SEM of 100 simulations for a 25×25 lattice. In all simulations, an initial perturbation of 1 was used. Lines represent the different widths of the gap-junctional conductance band in the step function model. (a) Widths of 100 mV, 80 mV, and 60 mV are shown in black, and widths of 40 mV and 20 mV are shown on a graded scale from dark to light; (b) Lines show widths of 60 mV, 40 mV, 39 mV, 38 mV, 30 mV, and 20 mV on a graded scale from dark to light. Activity is lost between widths of 40 mV and 39 mV.

(b)

Figure 5: The relationship between conductance and voltage difference for a selection of models. The solid blue and solid red lines represent the Miyoshi *et al.* [25] Type I and II models, respectively. (a) The green and yellow lines represent step function widths at the extremes of the critical range of values for total loss of excitability; (b) The blue and red dot-dashed lines represent widths outside of the critical range, chosen to coincide with the mid-points of conductances of the Type I and Type II models, respectively.

Figure 6: The relationship between the proportion of cells that become excited, and the ratio of Type I gap junctions (*i.e.* excitation possible) to Type II gap junctions (*i.e.* excitation impossible), for a smoothed step function model. Lines show probabilities of connections existing between any two cells of 1, 0.8, 0.6, and 0.4 on a graded scale from dark to light. Points show mean ± SEM of 100 simulations for a 25 × 25 lattice, all with an initial perturbation of 1.

Figure 7: Three-dimensional illustration of the network activity (relative cluster size) with varying connectivity p and proportion of Type I and Type II gap junctions. Each point in the mesh represents the mean of 100 simulations for a 25 × 25 lattice with an initial perturbation of 1. The density of the grid indicates that a larger proportion of cells are able to become excited with higher connectivity, and a greater proportion of Type I gap junctions than Type II gap junctions.

(b)

Figure 8: Relative cluster size versus connectivity p for a dynamic coupled lattice which relaxes back to the steady state in a fixed time period represented by different lines. Points show mean ± SEM of 100 simulations for a 25 × 25 lattice. In all simulations, an initial perturbation of 1 was used. The lines represent different time constant values. (a) Type I gap junctions. Lines represent time constants of 1 s, 0.5 s, and 0.1 s all shown in black due to their close proximity; (b) Type II gap junctions. Lines represent time constants of 1 s, 0.9 s, 0.7 s, 0.5 s, and 0.1 s on a graded scale from dark to light.

Figure 9: The relationship between the proportion of cells that become excited, and the ratio of Type I gap junctions to Type II gap junctions, for a model with dynamic gap-junctional conductances. Lines show probabilities of connections existing between any two cells of 1, 0.8, 0.6, 0.4, and 0.2 on a graded scale from dark to light. Points show mean ± SEM of 100 simulations for a 25 × 25 lattice, with an initial perturbation of 1.

(a) (b)

Figure 10: Gene expression of (a) connexin45 (Cx45) in the inner and outer myometrium; (b) connexin43 (Cx43) in the inner and outer myometrium at rat gestation days of 19.25 and 22 (in labour, LAB). Lines show the mean gene expression ± SD with $n = 3$ for gestation day 19.25 and $n = 2$ for gestation day 22 (LAB).

7 Tables

Table 1: Parameter values used in Equations 1a and 1b in all simulations.

Parameter	B	α	γ	w_0	v_0	ϵ
Value	3	3	0.05	0.4	0.4	0.2

Table 2: Parameter values for Equation 3.

	Negative V_j			Positive V_j		
	$G^-_{\min}$	V^-_h (mV)	A^- (mV^{-1})	$G^+_{\min}$	V^+_h (mV)	A^+ (mV^{-1})
Type I	0.34	-58.5	0.08	0.32	64.4	-0.07
Type II	0.26	-24.6	0.23	0.23	27.3	-0.11

Table 3: Summary of the excitation threshold time constants for Type II gap junctions.

Time constant (model units)	**Time constant (seconds)**	**Result**
$t \geqslant 1$	$\tau \geqslant 1.162$	Sigmoidal shape
$0.1 \leqslant t \leqslant 0.9$	$0.116 \leqslant \tau \leqslant 1.046$	Bell shape
$t < 0.1$	$\tau < 0.116$	No activity

8 Short Title

Cx43:45 ratio controls excitability

Appendix – Derivation of the FitzHugh-Nagumo model

We follow the derivation provided by Keener and Sneyd [28]. Consider the circuit given in Figure SI 2b showing a simplified model of the cell membrane. From Kirchoff's laws one obtains:

$$C_m \frac{dV}{d\tau} + F(V) + i = -I_0, \tag{7a}$$

$$D\frac{di}{d\tau} + Ri = V - V_0 \, , \tag{7b}$$

where I_0 is the applied external current, i is the current through the resistor-inductor, $V = V_i - V_e$ is the membrane potential, R is the resistance and V_0 is the potential gain across the battery which forms part of the excitable element representing the recovery current in Figure SI 2b. D is the damping coefficient, which captures the inertia of the system induced by the gating kinetics, as shown by FitzHugh in 1961 [14]. R and D are incorporated into the "excitable element". Here, τ represents dimensional time. The function $F(V)$ is a cubic with three zeros: the smallest $V = 0$ and largest $V = V_1$ are stable solutions of $dV/d\tau = -F(V)$. The passive resistance of the nonlinear element (defined as a tunnel diode by Nagumo [15]) is $R_1 = 1/F'(0)$.

The equations are rendered dimensionless as follows. Define $v = V/V_1$, $w = R_1 i/V_1$, $f(v) = -R_1 F(V_1 v)/V_1$ and $t = R_1\tau/L$. Equations (7) can then be rewritten as follows:

$$\epsilon \frac{dv}{dt} = f(v) - w - w_0, \tag{8a}$$

$$\frac{dw}{dt} = v - \gamma w - v_0, \tag{8b}$$

where $\epsilon = R_1^2 C_m/D$, $w_0 = R_1 I_0/V_1$, $v_0 = V_0/V_1$ and $\gamma = R/R_1$. The function $f(v)$ is a cubic and can be written as follows:

$$f(v) = Av(v-\alpha)(1-v) \, . \tag{9}$$

Supplementary Information

SI 1.1 Detailed experimental methods

We employed rat models in order to verify the changes in gene expression as pregnancy progresses. Our main objective was to ascertain whether the expression of Cx43 and Cx45 is consistent with the findings by Miyoshi *et al.* [25].

SI 1.1.1 Rat models

Twelve Sprague-Dawley rats (Harlan Laboratories) were used. Three animals were killed on gestational days $19\frac{1}{4}$, 20, and 22, respectively. In the latter case, a further distinction was drawn between animals that had begun labour (and had already delivered one pup) and those that were yet to enter it. Whole-uterine samples consisting of pups, uterine horns, and cervixes were flash frozen in liquid nitrogen stored at $-80°$C.

SI 1.1.2 Tissue Sectioning

Sections of 8 μm in thickness were cut on a cryostat ($-30°$C) and each section was adhered to a membrane slide (Molecular Machines & Industries).

SI 1.1.3 Tissue staining

Staining was performed using the Life Technologies LCM Staining kit using a 7:3 ratio mix of ethanolic solutions of Cresyl Violet (CV) nuclear stain and Eosin Yellow (EY) cytoplasmic stain (Sigma Aldrich), respectively. Slides were subsequently dehydrated through graded alcohols and transferred into a chamber containing xylene for 5 minutes. The slides were then desiccated for 5 minutes.

SI 1.1.4 Laser-capture microdissection

LCM was performed using the mmiCellCut® laser-capture microdissection system (Molecular Machines & Industries). Inner circular and outer longitudinal myometrial tissues were obtained separately, where care was taken to avoid blood vessels and glands. Microdissected tissue sections were collected using 500 μL mmi Isolation® tubes with adhesive lid and diffuser. Acquisition time was kept below 30 minutes.

SI 1.1.5 RNA isolation from LCM tissue sections

Total RNA was extracted from the LCM tissues using the Life Technologies RNAqueous®-Micro kit according to manufacturer instruction.

SI 1.1.6 RNA quantity and quality check

RNA was quantitated using the Thermo Scientific NanoDrop® 1000 Spectrophotometer and checked for quality by an Agilent 2100 Bioanalyzer and the Agilent RNA 6000 Pico kit according to manufacturer instruction.

SI 1.1.7 Library preparation and sequencing

RNA of acceptable quality, RIN $\geq$ 6, was used to create cDNA. The cDNA was amplified using the Nugen Ovation RNA-Seq System V2 according to the manufacturer's instructions. The Nugen Ovation Ultralow DR Multiplex System (1–8) was used for library preparation according to manufacturer's instructions. Libraries were validated using a DNA 1000 chip on an Agilent 2100 Bioanalyzer according to manufacturer's instructions. Libraries were sequenced on the Illumina HiSeq 2500 platform (Illumina, San Diego, CA, USA) using a 51 bp paired-end indexed run.

SI 1.1.8 Data quality assessment and analysis

The 51 bp paired-end sequencing reads were inspected for low quality scores, adapter sequence contamination, and other overrepresented sequences, using FASTQC [58]. TopHat 2.0.9 [59] was used to align reads of acceptable quality against the UCSC *Rattus norvegicus* (rn5) reference transcriptome from Illumina iGenomes [60]. The mapped reads were sorted and indexed using SAMtools-0.1.19 [61], to prepare data for the Integrative Genomics Viewer (IGV) [62].

Sailfish-0.6.2 [63] was used to used to estimate transcript abundance in the form of transcripts per million (TPM) [64], using the following equation:

$$\mathrm{TPM} = \frac{\mathrm{r_g} \times \mathrm{rl} \times 10^6}{\mathrm{fl_g} \times \mathrm{T}}, \tag{10}$$

where $\mathrm{r_g}$ represents the number of reads mapping to feature g, rl represents the mean feature length, $\mathrm{fl_g}$ represents the length of feature g, and T is the total number of mappable reads.

In order to detect the change in gene expression in the transition from pregnancy to labour, comparisons were made between the mean TPMs for connexin43 (Cx43) and connexin45 (Cx45) at gestational days 19.25 and 22 (in labour). The inner and outer myometrial layers were considered separately.

(a)

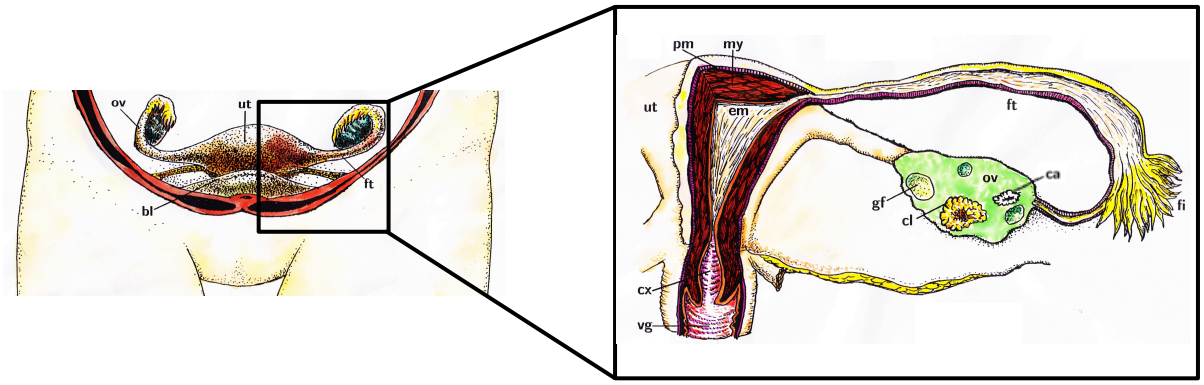

(b)

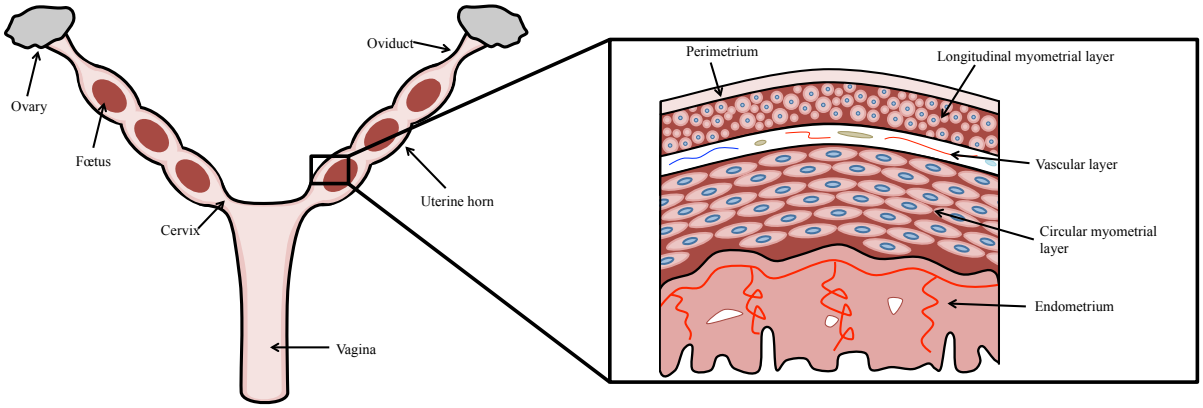

Figure SI 1: (a) Anatomy of the human female reproductive system. Left: location in the lower abdomen; Right: partially dissected uterus showing the layers of the uterine wall and the Fallopian tube. The following structures are indicated: **ut**: uterus; **ov**: ovary; **ft**: Fallopian tube; **bl**: bladder; **pm**: perimetrium; **my**: myometrium; **em**: endometrium; **gf**: Graafian follicle; **cl**: corpus luteum; **ca**: corpus albicans; **cx**: cervix; **vg**: vagina; (b) Anatomy of the rat reproductive system. Left: The rat uterus is divided into two horns. Fœtuses implant in the wall of each horn. Right: Cross-section of the uterine wall showing the outer perimetrium; the external, longitudinal myometrial layer; the vascular layer; the inner, circular myometrial layer; and the endometrium.

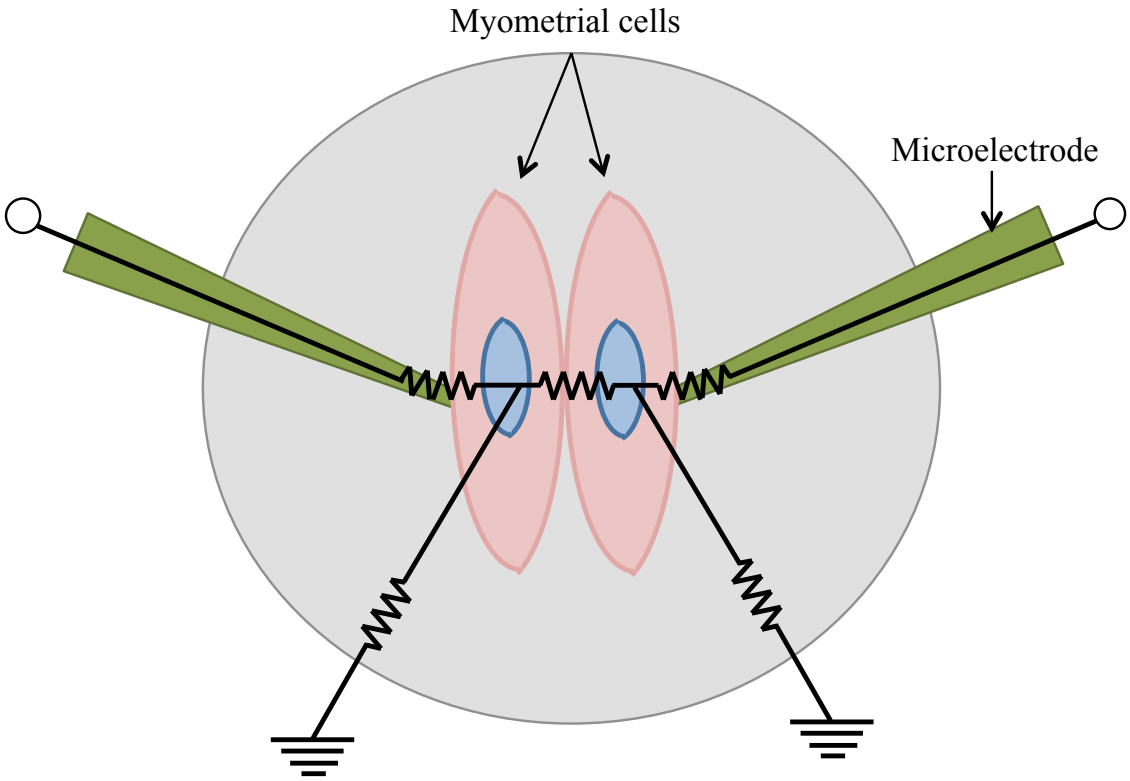

Figure SI 2: The two-microelectrode double patch-clamp set-up used by Miyoshi *et al.* [25] to measure the conductance across a gap junction. Two electrotonically coupled cells have been isolated and each has been patched by a microelectrode. The equivalent circuit is indicated: the resistor between the cells represents the gap junction, the resistors between the microelectrodes and cells are the electrode resistances, and the remaining resistors are the membrane (leak) conductances.

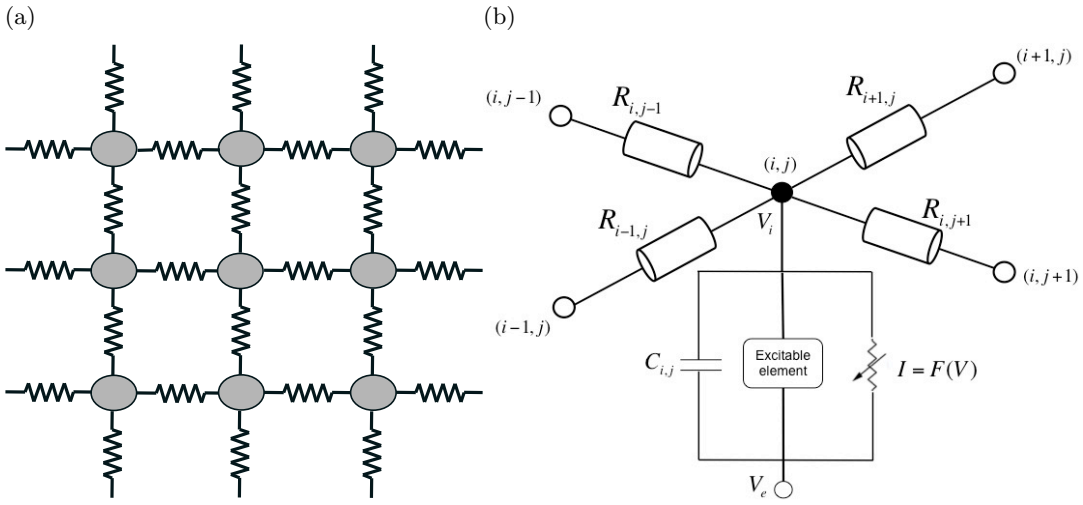

Figure SI 3: (a) Diagram of the model network. Each cell is represented by a circular node, and is connected to its four neighbours through resistors representing the gap junctions; (b) Electrical circuit diagram representing the current flow between connected cells. Cell (i, j) is the cell of interest, coupled to four surrounding cells; R represents the resistances in gap junctions. The circuit at cell (i, j) represents a basic model of an excitable system [28]. V_e represents the external potential; V_i represents the internal potential; $C_{i,j}$ is the cell capacitance; the excitable element represents the recovery current; and the non-linear current-voltage device (I) represents the fast current.

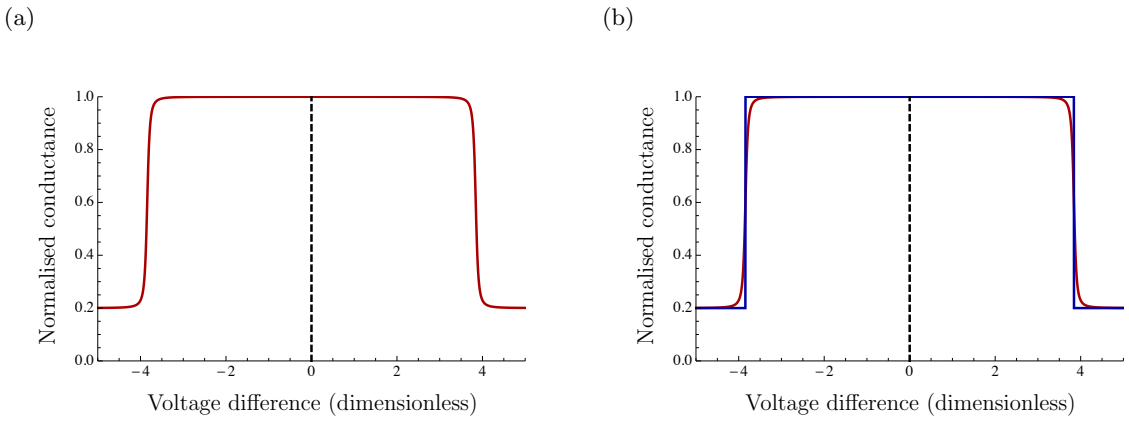

Figure SI 4: (a) Step function describing the relationship between voltage difference and gap-junctional conductance approximated by the sigmoidal equation given in Equation 2; (b) Step function (blue) overlayed with the approximated sigmoidal function (red).

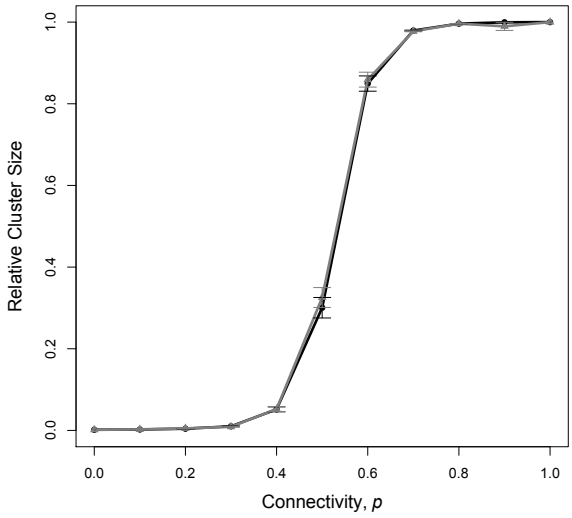

Figure SI 5: Relative cluster size versus connectivity p, comparing the infinite width step function model (shown in black) with the uniformly coupled Bernoulli model with $\kappa = 1$ previously published [13] (shown in grey). Points show mean ± SEM of 100 simulations for a 25×25 lattice, with an initial perturbation of 1.

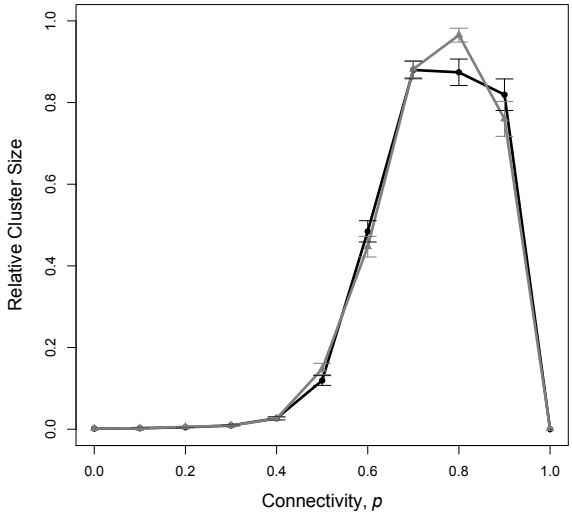

Figure SI 6: Relative cluster size versus connectivity p, comparing the infinite width step function model (shown in black) with the uniformly coupled Bernoulli model with coupling strength $\kappa = 0.76$ previously published [13] (shown in grey). Points show mean ± SEM of 100 simulations for a 25×25 lattice, with an initial perturbation of 1.

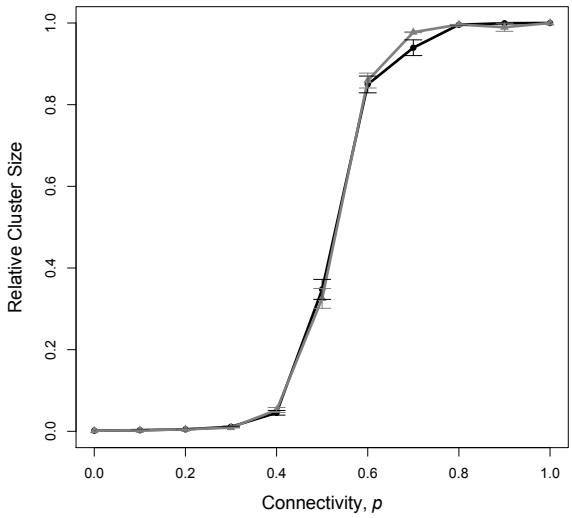

Figure SI 7: Relative cluster size versus connectivity p, comparing the infinite width symmetrical Miyoshi *et al.* [25] model (shown in black) with the uniformly coupled Bernoulli model previously published [13] (shown in grey). Points show mean ± SEM of 100 simulations for a 25×25 lattice, with an initial perturbation of 1.

(a) (b)

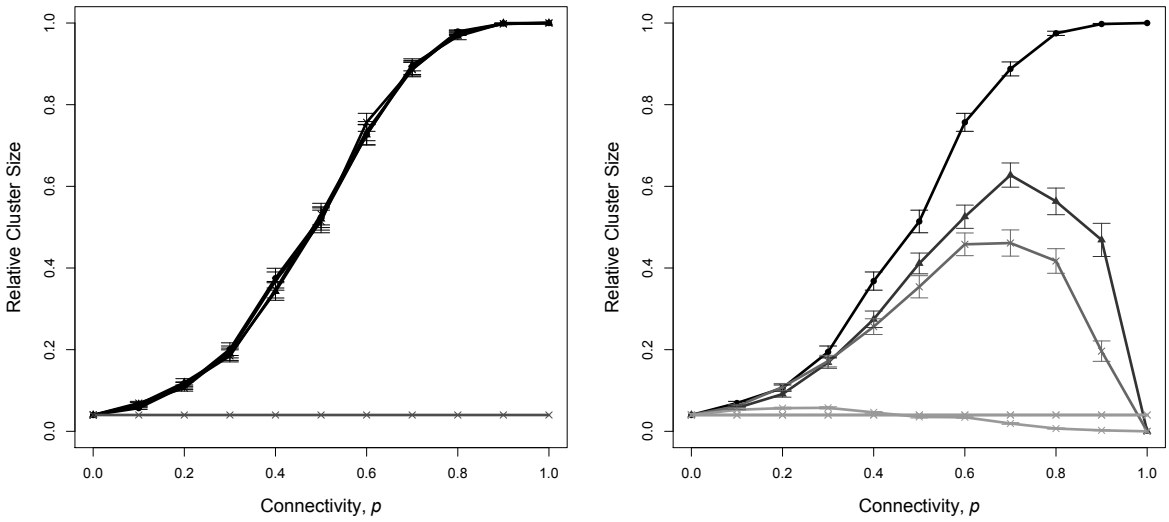

Figure SI 8: Relative cluster size versus connectivity for a lattice with gap-junctional conductance related to voltage-dependence with a step function. Points show mean ± SEM of 100 simulations for a 5 × 5 lattice. In all simulations, an initial perturbation of 1 was used. Lines represent the different widths of the gap-junctional conductance band in the step function model. (a) Widths of 100 mV, 80 mV, 60 mV, and 40 mV are shown in black, and a width of 20 mV is shown in grey; (b) Lines show widths of 40 mV, 39 mV, 38 mV, 35 mV, 30 mV, and 20 mV on a graded scale from dark to light.

(a) (b)

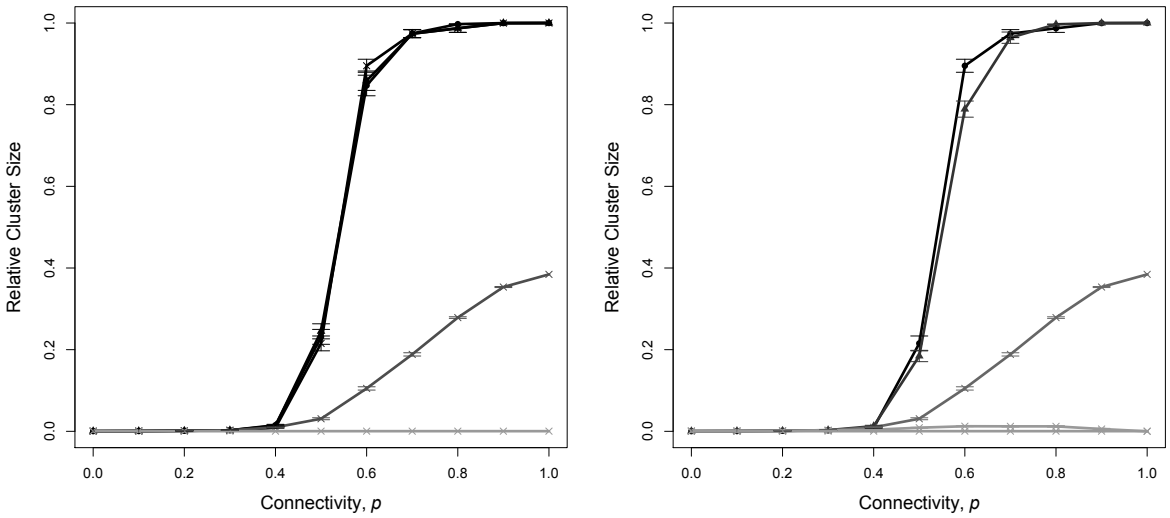

Figure SI 9: Relative cluster size versus connectivity for a lattice with gap-junctional conductance related to voltage-dependence with a step function. Points show mean ± SEM of 100 simulations for a 50 × 50 lattice. In all simulations, an initial perturbation of 1 was used. Lines represent the different widths of the gap-junctional conductance band in the step function model. (a) Widths of 100 mV, 80 mV, and 60 mV are shown in black, and widths of 40 mV and 20 mV are shown in shades of grey from dark to light; (b) Widths of 60 mV, 41 mV, 40 mV, 39 mV, and 20 mV are shown on a graded scale from dark to light.

(a) (b)

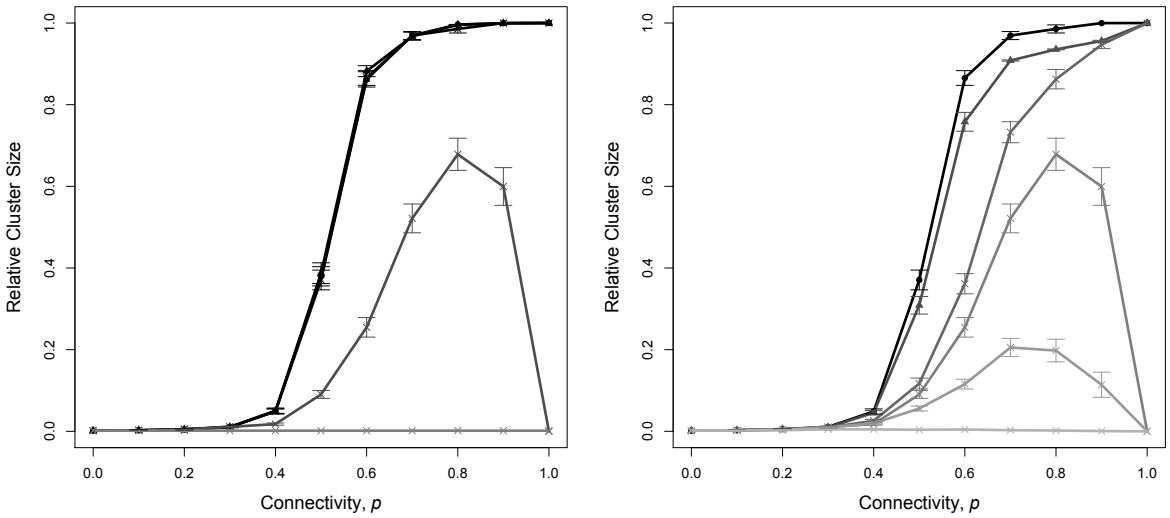

Figure SI 10: Relative cluster size versus connectivity p for a lattice with gap-junctional conductance related to voltage-dependence using a symmetrical Miyoshi *et al.* [25] relationship. Points show mean ± SEM of 100 simulations for a 25 × 25 lattice. In all simulations, an initial perturbation of 1 was used. Lines represent the different widths of the gap-junctional conductance band in the step function model. (a) Widths of 100 mV and 80 mV are shown in black, and widths of 60 mV, 40 mV, and 20 mV are shown in grey; (b) Lines show widths of 60 mV, 45 mV, 42 mV, 40 mV, 38 mV, and 35 mV on a graded scale from dark to light.

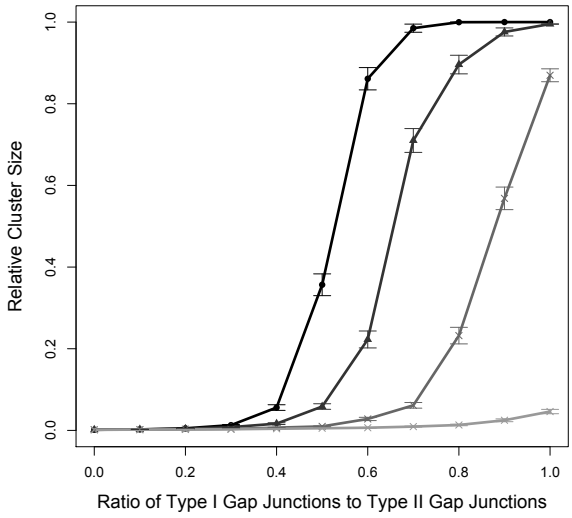

Figure SI 11: The relationship between the proportion of cells that become excited, and the ratio of Type I gap junctions (*i.e.* excitation possible) to Type II gap junctions (*i.e.* excitation impossible), for a symmetrical Miyoshi *et al.* [25] model. Lines show probabilities of connections existing between any two cells of 1, 0.8, 0.6, and 0.4 on a graded scale from dark to light. Points show mean ± SEM of 100 simulations for a 25 × 25 lattice, all with an initial perturbation of 1.

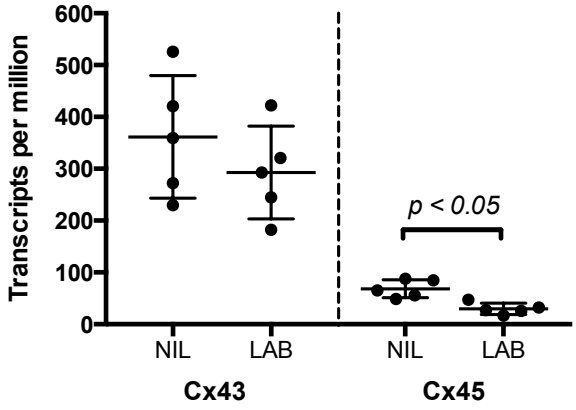

Figure SI 12: The gene expression of connexin45 and connexin43 in "in labour" human myometrial samples (LAB) compared with "not-in-labour" human myometrial samples taken at term (NIL). Lines show the mean gene expression ± SD of 5 samples. There is no significant change in connexin43 between the non-labour and labour samples. There is a significant decrease in connexin45 expression in labour when compared with non-labour ($p = 0.0030$). Graph created from data published by Chan *et al.* [36].